

Polarization effects in diffraction-induced laser pulse splitting in one-dimensional photonic crystals

Sergey E. Svyakhovskiy,¹ Alexander A. Skorynin,¹ Vladimir A. Bushuev,¹ Sergey V. Chekalin,²
Victor O. Kompanets,² Anton I. Maydykovskiy,¹ Tatiana V. Murzina,¹
Vladimir B. Novikov,¹ and Boris I. Mantsyzov^{1,*}

¹Department of Physics, M. V. Lomonosov Moscow State University, Moscow 119991, Russia

²Institute of Spectroscopy RAS, Fizicheskaya Street 5, Troitsk, Moscow Region 142190, Russia

*Corresponding author: bmantsyzov@gmail.com

Received January 4, 2013; accepted February 28, 2013;
posted March 20, 2013 (Doc. ID 182597); published April 19, 2013

The polarization effects in the diffraction-induced pulse splitting (DIPS) observed under the dynamical Bragg diffraction in the Laue geometry in linear one-dimensional photonic crystals (PCs) are studied theoretically and experimentally. It is demonstrated that the characteristic length of the laser pulse path in a PC, or splitting length, used to describe the temporal pulse splitting, as well as the number of the outgoing femtosecond pulses, are influenced significantly by the polarization of the incident laser pulse. We have observed that the characteristic splitting time in porous quartz PCs for the *s*-polarized probe pulse is approximately 1.5 times smaller as compared with that measured for the *p*-polarized radiation. These results are supported by the theoretical description and ensure that the polarization sensitivity of the DIPS effect is due to a large lattice-induced dispersion of the PC. It is also shown that the number of output pulses can be varied from two up to four in both transmission and diffraction directions depending on the polarization of incident femtosecond pulses. © 2013 Optical Society of America

OCIS codes: (050.1960) Diffraction theory; (050.5298) Photonic crystals; (350.4238) Nanophotonics and photonic crystals; (350.5500) Propagation.

<http://dx.doi.org/10.1364/JOSAB.30.001261>

1. INTRODUCTION

Photonic crystals (PCs) that are spatially periodic structures with the period comparable with the wavelength of light have been intensively studied in last two decades. They reveal a number of novel optical effects that are prospective for the development of new methods for the operation over the parameters and the dynamics of laser pulses [1–3]. Thus, it has been demonstrated that the propagation of laser pulses with a wavelength that is close to the spectral edge of the photonic band gap results in a strong localization of light within the structure [4] and in a drastic decrease of the group velocity (“slow light”) [5–7]. As a direct consequence of these effects, a significant amplification of the efficiency of the nonlinear-optical effects in PC structures [8,9], as well as the decrease of the excitation threshold in PC-based lasers [10], was achieved. It has been shown that the so-called gap solitons can exist under the nonlinear interaction of laser pulses with PCs [2,11]. The gap solitons are the nonlinear solitary waves that propagate at the frequency within the linear photonic band gap and that keep their shape and energy during the propagation and after the interaction. The pendular effect, i.e., a periodic oscillation of the energy between propagation and diffraction in a PC wave, was also observed in PC structures [12–15]. This effect is of special interest for an all-optical switching of laser pulses propagating in a PC. Recently, a novel optical diffraction phenomenon of diffraction-induced laser pulses splitting (DIPS) under the dynamical Bragg diffraction in the Laue scheme of diffraction in a linear one-dimensional (1D) PC was described theoretically [16,17] and then observed experimentally [18]. In that case, the laser

pulses are incident on the structure as is shown in Fig. 1 and propagate within a PC under the Bragg diffraction condition parallel to the layers. It was shown [16–18] that, in this case, a laser pulse inside a PC can be split into two pulses that correspond to the two eigenmodes of the electromagnetic field inside a PC, the so-called Borrmann and anti-Borrmann optical modes. The first one is localized predominantly inside the layers with smaller value of the refractive index, while the latter one is localized in those with larger refractive index. Consequently, the pulses of these modes propagate within a PC with different group velocities and, thus, a temporal splitting of a short incident laser pulse can be observed. At the same time, the effect of the polarization of incident radiation on the DIPS effect has not been studied.

In this paper the polarization effects in diffraction-induced pulse splitting (DIPS) in porous-quartz-based 1D linear PCs under the dynamical Bragg diffraction in the Laue geometry are studied both experimentally and theoretically. We demonstrate that the difference in the group velocity of the Borrmann and anti-Borrmann modes is substantially different for the *p*- and *s*-polarized pulsed radiation due to a large lattice-induced dispersion in a PC. This leads to a significant change in the value of the temporal splitting for *p*- and *s*-polarized laser pulses propagating within a PC and, in general, in the number of the outgoing pulses as well. After passing a PC the number of outgoing pulses can be varied from two up to four in both transmission and diffraction directions, depending on the polarization of the incident radiation and the parameters of a PC. We also show that an important point here is that, due to a large value of the lattice-induced dispersion in

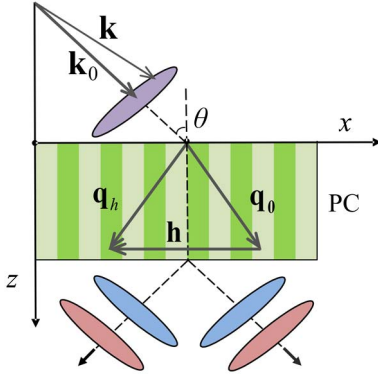


Fig. 1. Schematic diagram of the diffraction-induced pulse splitting within 1D PC at the Bragg diffraction in the Laue geometry.

the PC, not only the first term in the expansion of the polarization factor should be considered but the second one as well, which describes the unusual polarization dependence of the DIPS effect. The results of the theoretical description stay in a good agreement with obtained experimental data for a 1D porous quartz multilayer PC.

2. DYNAMICAL DIFFRACTION OF A LINEAR POLARIZED LASER PULSE IN A PC AT THE LAUE SCHEME OF DIFFRACTION (THEORY)

Let us consider a 1D PC that consists of optically isotropic, periodically alternating layers of the thicknesses d_1 , d_2 and refractive indices n_1 , n_2 oriented perpendicularly to the PC surface (Fig. 1). A spatially confined light pulse is incident on the PC at an angle θ to the normal to its surface; the electric field of the pulse is described by

$$\mathbf{E}_{\text{in}}(\mathbf{r}, t) = \mathbf{e}_{\text{in}} E_{\text{in}}(\mathbf{r}, t) \exp(i\mathbf{k}_0 \mathbf{r} - i\omega_0 t), \quad (1)$$

where $E_{\text{in}}(\mathbf{r}, t)$ is the slowly varying complex amplitude, \mathbf{e}_{in} is the unit vector of the polarization plane, ω_0 is the central frequency and $k_0 = |\mathbf{k}_0| = \omega_0/c = 2\pi/\lambda_0$, λ_0 is the central wavelength of the optical pulse, c is the speed of light in vacuum, projections of the central wave vector \mathbf{k}_0 are $k_{0x} = k_0 \sin \theta$, $k_{0z} = k_0 \cos \theta$, and the x and z axes lie in the plane of incidence and are directed parallel and perpendicularly to the PC surface, respectively, as is shown in Fig. 1. For simplicity, we consider the parameters of the laser pulse and of the PC structure to be constant along the y axis.

Under these conditions the field of the incident pulse [Eq. (1)] at the PC surface ($z = 0$) can be represented as a two-dimensional (2D) Fourier decomposition, i.e., as a set of plane monochromatic waves with the amplitudes $\mathbf{E}_{\text{in}}(k_x, \omega)$, frequencies $\omega = \omega_0 + \Omega$, and wave vectors \mathbf{k} , where $|\mathbf{k}| \equiv k = \omega/c$, the \mathbf{k} projections being defined by $k_x = k_{0x} + K$, $k_z = [(\omega/c)^2 - k_x^2]^{1/2}$:

$$\mathbf{E}_{\text{in}}(x, t) = \int_{-\infty}^{\infty} \int_{-\infty}^{\infty} \mathbf{E}_{\text{in}}(k_x, \omega) \exp(ik_x x - i\omega t) dk_x d\omega, \quad (2)$$

where the spectral frequency-angular amplitudes, for example, in the case of s-polarization are

$$\begin{aligned} \mathbf{E}_{\text{in}}(k_x, \omega) &= \mathbf{e}_{\text{in}} E_{\text{in}}(k, \Omega) \\ &= \mathbf{e}_{\text{in}} \frac{1}{4\pi^2} \int_{-\infty}^{\infty} \int_{-\infty}^{\infty} E_{\text{in}}(x, t) \exp(-iKx + i\Omega t) dx dt. \end{aligned} \quad (3)$$

The complex field $\mathbf{E}(\mathbf{r}, t)$ in a dielectric nonmagnetic PC obeys the wave equation

$$\nabla \times \nabla \times \mathbf{E}(\mathbf{r}, t) + \frac{\varepsilon(x)}{c^2} \frac{\partial^2 \mathbf{E}(\mathbf{r}, t)}{\partial t^2} = 0, \quad (4)$$

where ∇ is the Nabla operator and $\varepsilon(x) = n^2(x)$ is the complex permittivity that is spatially modulated within a PC. We will represent the refractive index of the medium $n(x)$ in a PC as

$$n(x) = n_a + \Delta n(x),$$

where the average refractive index is introduced as

$$n_a = (n_1 d_1 + n_2 d_2)/d = n_2 + \xi \delta,$$

$\delta = n_1 - n_2$ being the modulation of the refractive index, $\xi = d_1/d$, and $d = d_1 + d_2$ is the period of the structure. The function $\Delta n(x)$ is $\Delta n(x) = (1 - \xi)\delta$ in the layers of the thickness d_1 and $\Delta n(x) = -\xi\delta$ in the layers of the thickness d_2 .

The left-hand part of Eq. (4) is $\nabla \times \nabla \times \mathbf{E}(\mathbf{r}, t) = -\Delta \mathbf{E}(\mathbf{r}, t) + \nabla(\nabla \mathbf{E}(\mathbf{r}, t))$, where $\Delta = \partial^2/\partial x^2 + \partial^2/\partial z^2$ is the Laplace operator, and $\nabla \mathbf{E} = -\varepsilon^{-1}(\nabla \varepsilon) \mathbf{E}$. The gradient $\nabla \varepsilon \neq 0$ in a structure with spatially modulated permittivity $\varepsilon(\mathbf{r})$, therefore, the field divergence $\nabla \mathbf{E} \neq 0$ and a plane electromagnetic wave with arbitrary polarization is not transverse. In other words, the vector \mathbf{E} has a nonzero projection on a wave vector. In that case, it is more convenient to pass on from Eq. (4) to the wave equation for the magnetic field $\mathbf{H}(\mathbf{r}, t)$, which is transverse in a non-magnetic medium so that the wave equation takes the form

$$\Delta \mathbf{H}(\mathbf{r}, t) + \frac{\nabla \varepsilon}{\varepsilon} \times \nabla \times \mathbf{H}(\mathbf{r}, t) - \frac{\varepsilon(x)}{c^2} \frac{\partial^2 \mathbf{H}(\mathbf{r}, t)}{\partial t^2} = 0. \quad (5)$$

Let us consider the case of a narrow enough spectrum of the incident pulse [Eq. (3)], when the spectrum is within the Bragg frequency band, and assume that the central frequency ω_0 is close to the fulfillment of the Bragg condition $2k_0 \sin \theta_B = h$, where $h = |\mathbf{h}| = 2\pi/d$ is the magnitude of the reciprocal lattice vector \mathbf{h} , and θ_B is the Bragg angle for radiation with a central frequency ω_0 . Then the diffraction can be described within a two-wave approximation when the electromagnetic waves inside a PC are represented by two “strong” waves—the transmitted and diffracted ones—with the wave vectors \mathbf{q}_0 and $\mathbf{q}_h = \mathbf{q}_0 + \mathbf{h}$ for each spectral frequency-angular field component. Thus, the total field inside a 1D PC is a coherent superposition of the transmitted ($\mathbf{H}_0, \mathbf{E}_0$) and diffracted ($\mathbf{H}_h, \mathbf{E}_h$) pulse fields:

$$\begin{aligned} \mathbf{H}(\mathbf{r}, t) &= \mathbf{H}_0(\mathbf{r}, t) + \mathbf{H}_h(\mathbf{r}, t), \\ \mathbf{E}(\mathbf{r}, t) &= \mathbf{E}_0(\mathbf{r}, t) + \mathbf{E}_h(\mathbf{r}, t). \end{aligned} \quad (6)$$

The magnetic component of the electromagnetic field in a PC can be presented in the form of a 2D Fourier decomposition:

$$\mathbf{H}_g(x, z, t) = \int_{-\infty}^{\infty} \int_{-\infty}^{\infty} \mathbf{H}_g(K, \Omega) \times \exp[i(q_{0x} - g)x + iq_z z - i\omega t] dK d\Omega, \quad g = 0, h, \quad (7)$$

i.e., as a set of plane monochromatic waves with the spectral amplitudes $\mathbf{H}_{0,h}(K, \Omega)$ and wave vectors $\mathbf{q}_0 = q_{0x}\mathbf{e}_x + q_z\mathbf{e}_z$ and $\mathbf{q}_h = \mathbf{q}_0 + \mathbf{h} = (q_{0x} - h)\mathbf{e}_x + q_z\mathbf{e}_z$, where $\mathbf{h} = -h\mathbf{e}_x$. Here \mathbf{e}_i are the unit vectors of the coordinate axes. A similar expression can be written for the electric component of the field $\mathbf{E}_{0,h}(x, z, t)$ with the spectral amplitudes $\mathbf{E}_{0,h}(K, \Omega)$. The x projections of the wave vectors q_{0x} in Eq. (7) are determined from continuity of the tangential components of the wave vectors $q_{0x} = k_x = k_{0x} + K$ on the surface of the PC (at $z = 0$). The z projections $q_z = q_z(K, \Omega)$ of the wave vectors are determined from Eq. (5).

Let us consider the solution of the wave equation [Eq. (5)] in the two-wave approximation [Eq. (6)]. Periodical functions in the second and third terms of Eq. (5) can be expanded in Fourier series in the reciprocal lattice vectors. When keeping the terms in the series that correspond to the two-wave approximation [19], the permittivity $\varepsilon(x)$ takes the form

$$\varepsilon(x) = \chi_0 + \chi_h \exp(-ihx) + \chi_{-h} \exp(ihx), \quad (8)$$

where χ_0 , χ_h , and χ_{-h} are the Fourier components of the permittivity:

$$\chi_g = \frac{1}{d} \int_0^d \varepsilon(x) \exp(igx) dx, \quad g = 0, h, -h,$$

which are defined for a multilayer structure by the relations

$$\begin{aligned} \chi_0 &= n_a^2 + \delta^2(\xi - \xi^2), \\ \chi_h &= \frac{i}{\pi} \left(n_a \delta + \delta^2 \frac{1 - 2\xi}{2} \right) [1 - \exp(i2\pi\xi)], \\ \chi_{-h} &= -\frac{i}{\pi} \left(n_a \delta + \delta^2 \frac{1 - 2\xi}{2} \right) [1 - \exp(-i2\pi\xi)]. \end{aligned}$$

It should be emphasized that the quantity $\eta = \chi/\chi_0$ ($\chi \equiv |\chi_{\pm h}|$) is a small parameter $\eta \ll 1$ even if the modulation of the refractive index is quite significant, $\delta < 0.3$ and $n_a > 1.3$, which is close to the experimental conditions discussed in the next section.

By analogy with the expansion of $\varepsilon(x)$, the periodic function $\nu(x) \equiv \varepsilon(x)^{-1} \nabla \varepsilon(x)$ can also be presented as a series in the reciprocal lattice vectors. When keeping the terms in the series that correspond to the two-wave approximation we obtain the following expression:

$$\nu(x) = \mathbf{e}_x [\nu_0 + \nu_h \exp(-ihx) + \nu_{-h} \exp(ihx)], \quad (9)$$

where

$$\nu_g = \frac{1}{d} \int_0^d \frac{1}{\varepsilon(x)} \frac{\partial \varepsilon(x)}{\partial x} \exp(igx) dx, \quad g = 0, h, -h. \quad (10)$$

It is clear from Eq. (10) that $\nu_0 = 0$ for $g = 0$. In the case $g = \pm h$ the values of ν_g in Eq. (10) can be calculated in the first order on η :

$$\nu_h = -ih\chi_h/\chi_0, \quad \nu_{-h} = ih\chi_{-h}/\chi_0.$$

Thus, a system of vector equations for the magnetic field spectral amplitudes $\mathbf{H}_{0,h}(K, \Omega)$ (7) can be obtained by substituting Eqs. (6), (7), (8), and (9) into the wave equation [Eq. (5)]:

$$\begin{aligned} \beta \mathbf{H}_0 - \chi_{-h} \mathbf{H}_h - i\nu_{-h} \mathbf{e}_x \times \mathbf{q}_h \times \mathbf{H}_h/k^2 &= 0, \\ \chi_h \mathbf{H}_0 - (\beta - \alpha) \mathbf{H}_h + i\nu_h \mathbf{e}_x \times \mathbf{q}_0 \times \mathbf{H}_0/k^2 &= 0, \end{aligned} \quad (11)$$

where the following designations are introduced:

$$\begin{aligned} \beta &= (q_z^2 - k^2 \gamma^2)/k^2, & \gamma &= (k^2 \chi_0 - q_{0x}^2)^{1/2}/k, \\ \alpha &= h(2q_{0x} - h)/k^2, & k &= \omega/c. \end{aligned}$$

Here the quantity α defines the degree of detuning from the exact Bragg condition $\alpha = 0$.

The system of vector equations [Eq. (11)] is obtained for an arbitrary polarization of the incident light. In what follows two special cases of linear polarization are considered: s-polarization, when the electric field vector \mathbf{E}_{in} of an incident pulse is transverse to the plane of incidence (TE wave), and p-polarization when the magnetic field vector \mathbf{H}_{in} is transverse to the plane of incidence (TM wave).

A. P-Polarized Field

The magnetic field for the p-polarized radiation is $\mathbf{H}_g = \mathbf{e}_y H_g$, i.e., all the vectors in Eqs. (11) are parallel to the y axis, so the Eqs. (11) take the form

$$\beta H_0 - C_{-h} \chi_{-h} H_h = 0, \quad C_h \chi_h H_0 - (\beta - \alpha) H_h = 0, \quad (12)$$

where $C_h = 1 - i\nu_h q_{0x}/k^2 \chi_h$, $C_{-h} = 1 - i\nu_{-h}(q_{0x} - h)/k^2 \chi_{-h}$. A quadratic equation for the variable β is derived from the condition for the nontrivial solution of the system [Eq. (12)] for the amplitudes H_0 and H_h :

$$\beta(\beta - \alpha) - C_h C_{-h} \chi_h \chi_{-h} = 0,$$

which in turn gives the two values of β :

$$\beta_{1,2} = (1/2)[\alpha \mp (\alpha^2 + 4C_h C_{-h} \chi_h \chi_{-h})^{1/2}], \quad (13)$$

where the coefficients $C_{h,-h}$ for a multilayered structure and in the case of $\eta \ll 1$ are

$$C_h = 1 - hq_{0x}/k^2 \chi_0, \quad C_{-h} = 1 - h(h - q_{0x})/k^2 \chi_0. \quad (14)$$

The polarization factor $C = \sqrt{C_h C_{-h}}$ in Eq. (13) near the exact Bragg condition is $C \approx \cos \theta'$, where θ' is the angle between the vectors \mathbf{q}_0 and \mathbf{q}_h inside the PC. For an s-polarized field the polarization factor is $C = 1$ [see Eq. (24)].

When considering the waves propagating into the semi-infinite PC and taking into account Eq. (13), the following final expression for the z projections of the wave vectors in a PC can be obtained:

$$q_{zj} = k(\gamma^2 + \beta_j)^{1/2}, \quad j = 1, 2. \quad (15)$$

This is the dispersion equation for the electromagnetic waves in a 1D PC.

It follows from Eq. (15) that four waves inside a PC structure exist that correspond to each of the incident plane waves of the input pulse [Eq. (3)]: the two transmitted waves with the wave vectors $\mathbf{q}_{0j} = q_{0x}\mathbf{e}_x + q_{zj}\mathbf{e}_z$ and amplitudes $H_{0j}(K, \Omega)$ and two diffracted waves with the wave vectors $\mathbf{q}_{hj} = (q_{0x} - h)\mathbf{e}_x + q_{zj}\mathbf{e}_z$ and the amplitudes $H_{hj}(K, \Omega)$. These waves when acting in pairs form the two eigenmodes of the field inside a PC: the Borrmann ($j = 1$) and the anti-Borrmann ($j = 2$) modes, which are spatially localized in the layers with low and high refractive indexes, respectively [16,17]. The relation between the field amplitudes H_{hj} and H_{0j} stems from the first equation in Eq. (12):

$$H_{hj} = R_j H_{0j}, \tag{16}$$

where $R_j = \beta_j / C_{-h}\chi_{-h}$.

Let us now obtain the spectral amplitudes of the electric field components. The relation between the electric induction and field vectors in the two-wave approximation is defined by $\mathbf{D}_g = \sum_{g'=0,h} \mathbf{E}_{g'} \chi_{g-g'}$, thus,

$$\begin{aligned} \mathbf{E}_{0j} &= \frac{\mathbf{D}_{0j} - \mathbf{D}_{hj}\chi_{-h}/\chi_0}{\chi_0 - \chi^2/\chi_0}, \\ \mathbf{E}_{hj} &= \frac{\mathbf{D}_{hj} - \mathbf{D}_{0j}\chi_h/\chi_0}{\chi_0 - \chi^2/\chi_0}. \end{aligned} \tag{17}$$

It stems from Eq. (17) that the vectors \mathbf{E}_{gj} and \mathbf{D}_{gj} are non-collinear, while the angle φ between them near the Bragg condition is small, as $\sin \varphi \approx \eta \sin 2\theta_B \ll 1$ if $\eta \ll 1$. The directions of the electric induction vectors $\mathbf{D}_{gj} = \mathbf{d}_{gj} D_{gj}$ are specified by the unit vectors $\mathbf{d}_{gj} = (q_{zj}/q_{gj})\mathbf{e}_x - [(q_{0x} - g)/q_{gj}]\mathbf{e}_z$, where $q_{gj} = [(q_{0x} - g)^2 + q_{zj}^2]^{1/2}$, and their amplitudes in accordance with the Maxwell equation $\nabla \times \mathbf{H} = c^{-1} \partial \mathbf{D} / \partial t$ are connected with the amplitudes of magnetic field H_{gj} as

$$D_{gj} = q_{gj} H_{gj} / k. \tag{18}$$

The following expressions for the electric field amplitudes are obtained by substituting Eq. (18) into Eq. (17) and when considering the terms of the first order in η :

$$\begin{aligned} E_{0j} &= \frac{q_{0j}}{k\chi_0} \left(1 - \frac{R_j \chi_{-h} q_{0j}^2 - q_{0x} h}{\chi_0 q_{0j}^2} \right) H_{0j}, \\ E_{hj} &= \frac{q_{hj}}{k\chi_0} \left(1 - \frac{\chi_h q_{0j}^2 - q_{0x} h}{R_j \chi_0 q_{hj}^2} \right) H_{hj}. \end{aligned} \tag{19}$$

The Fourier amplitudes of the fields H_{0j} can be determined from the boundary conditions for the tangential components of the magnetic H_y and the electric fields E_x at $z = 0$ taking into account Eqs. (17) and (18):

$$\begin{aligned} H_{in} + H_r &= H_{01} + H_{02}, & k_z (H_{in} - H_r) &= f_1 H_{01} + f_2 H_{02}, \\ R_1 H_{01} + R_2 H_{02} &= 0, \end{aligned} \tag{20}$$

where H_r is the amplitude of the specularly reflected wave, $f_j = (q_{zj}/\chi_0)(1 - R_j \chi_{-h}/\chi_0)$, the amplitudes of the electric and magnetic components of the input field are equal to each

other, $H_{in}(K, \Omega) = E_{in}(K, \Omega)$. The solution of the system [Eq. (20)] is given by:

$$H_{0j} = B_{0j} H_{in}, \tag{21}$$

where $B_{01} = -(1 + R_r)R_2/R_{12}$, $B_{02} = (1 + R_r)R_1/R_{12}$, and $R_{12} = R_1 - R_2$; $R_r = H_r/H_{in} = (k_z - f_r)/(k_z + f_r)$ is the Fresnel reflection coefficient modified by the diffraction in the layered structure, $f_r = (f_2 R_1 - f_1 R_2)/R_{12}$.

As a result, the following expression for the p -polarized magnetic fields of the transmitted and diffracted waves [Eq. (6)] in a 1D PC is found:

$$\begin{aligned} \mathbf{H}_g(x, z, t) &= \mathbf{e}_y \int_{-\infty}^{\infty} \int_{-\infty}^{\infty} B_g(K, \Omega, z) H_{in}(K, \Omega) \\ &\times \exp(iKx - i\Omega t) dK d\Omega \\ &\times \exp[i(k_{0x} - g)x - i\omega_0 t], \end{aligned} \tag{22}$$

where

$$B_g(K, \Omega, z) = \sum_{j=1,2} B_{gj} \exp(iq_{zj}z),$$

$B_{hj} = R_j B_{0j}$, and B_0 and B_h are the transmission and reflection amplitude coefficients of the plane waves in a PC layer of the thickness z , respectively.

B. S-Polarized Field

Let us consider now the diffraction of the s -polarized incident optical pulsed radiation, as the electric field vectors are parallel to the y axis, $\mathbf{E}_g = \mathbf{e}_y E_g$, so the x projections of the vector equations [Eqs. (11)] take the form:

$$\beta H_0 - \chi_{-h}(q_0/q_h)H_h = 0, \quad \chi_h(q_h/q_0)H_0 - (\beta - \alpha)H_h = 0.$$

Taking into account the relation between the amplitudes of the fields $H_g = q_g E_g / k$, the equations for the electric field amplitudes can be obtained:

$$\beta E_0 - \chi_{-h} E_h = 0, \quad \chi_h E_0 - (\beta - \alpha) E_h = 0. \tag{23}$$

It is easy to show that, much as in the case of p -polarization of the field, four waves occur in a PC for each plane wave component of the incident pulse field [16,17]. The expressions for the diffraction corrections $\beta_j^{(s)}$ in Eqs. (23) and the wave vector projections $q_{zj}^{(s)}$ can also be obtained from Eqs. (13) and (15) using the substitution $C_h = C_{-h} = 1$:

$$\begin{aligned} \beta_{1,2}^{(s)} &= (1/2)[\alpha \mp (\alpha^2 + 4\chi_h \chi_{-h})^{1/2}], \\ q_{zj}^{(s)} &= k(\gamma^2 + \beta_j^{(s)})^{1/2}, \quad j = 1, 2. \end{aligned} \tag{24}$$

Here the superscript “ s ” denotes the s -polarization of the incident field. An important point here is that the values $\beta_j^{(s)}$ and $q_{zj}^{(s)}$ [Eq. (24)] for the s -polarized waves differ from the analogous quantities obtained above for the p -polarized field [Eqs. (13) and (15)].

The Fourier amplitudes $E_{gj}^{(s)}$ are determined from the boundary conditions for the electric and magnetic components of the optical fields at $z = 0$ and for the case of s -polarization of the incident field:

$$\begin{aligned} E_{\text{in}} + E_r &= E_{01}^{(s)} + E_{02}^{(s)}, & k_z(E_{\text{in}} - E_r) &= q_{z1}^{(s)}E_{01}^{(s)} + q_{z2}^{(s)}E_{02}^{(s)}, \\ R_1^{(s)}E_{01}^{(s)} + R_2^{(s)}E_{02}^{(s)} &= 0. \end{aligned} \quad (25)$$

The solutions of Eqs. (25) are given by

$$E_{0j}^{(s)} = B_{0j}^{(s)}E_{\text{in}}, \quad (26)$$

where $B_{01}^{(s)} = -(1 + R_r^{(s)})R_2^{(s)}/R_{12}^{(s)}$, $B_{02}^{(s)} = (1 + R_r^{(s)})R_1^{(s)}/R_{12}^{(s)}$. The expression [Eq. (26)] with relations $E_{hj}^{(s)} = B_{hj}^{(s)}E_{\text{in}}$ defines the fields inside a 1D PC. Here the following coefficients are introduced: $B_{hj}^{(s)} = R_j^{(s)}B_{0j}^{(s)}$, $R_{12}^{(s)} = R_1^{(s)} - R_2^{(s)}$, $R_r^{(s)} = E_r/E_{\text{in}} = (k_z - f_r^{(s)})/(k_z + f_r^{(s)})$, and $f_r^{(s)} = (q_{z2}^{(s)}R_1^{(s)} - q_{z1}^{(s)}R_2^{(s)})/R_{12}^{(s)}$, similarly to Eq. (21).

Finally, the expression for the *s*-polarized fields of the transmitted and diffracted waves [Eq. (6)] propagating inside a PC takes the form

$$\begin{aligned} \mathbf{E}_g^{(s)}(x, z, t) &= \mathbf{e}_y \int_{-\infty}^{\infty} \int_{-\infty}^{\infty} B_g^{(s)}(K, \Omega, z) E_{\text{in}}(K, \Omega) \\ &\times \exp(iKx - i\Omega t) dK d\Omega \\ &\times \exp[i(k_{0x} - g)x - i\omega_0 t], \end{aligned} \quad (27)$$

where

$$B_g^{(s)}(K, \Omega, z) = \sum_{j=1,2} B_{gj}^{(s)} \exp(iq_{zj}^{(s)}z).$$

Here $B_0^{(s)}$ and $B_h^{(s)}$ are the transmission and reflection amplitude coefficients of the plane waves that propagate in a PC layer of the thickness z .

The total field [Eq. (6)] can also be represented as the sum of the Borrmann ($j = 1$) and anti-Borrmann ($j = 2$) field modes, the corresponding expression for the case of *s*-polarized incident radiation looks like

$$\mathbf{E}^{(s)}(x, z, t) = [\mathbf{E}_1^{(s)}(x, z, t) + \mathbf{E}_2^{(s)}(x, z, t)] \exp(ik_{0x}x - i\omega_0 t), \quad (28)$$

where

$$\begin{aligned} \mathbf{E}_j^{(s)}(x, z, t) &= \mathbf{e}_y \int_{-\infty}^{\infty} \int_{-\infty}^{\infty} B_j^{(s)}(K, \Omega, z) E_{\text{in}}(K, \Omega) \\ &\times \exp(iKx - i\Omega t) dK d\Omega, \quad j = 1, 2, \end{aligned}$$

$$B_j^{(s)}(K, \Omega, z) = \exp(iq_{zj}^{(s)}z) \sum_{g=0,h} B_{gj}^{(s)} \exp(-igx).$$

For the *p*-polarized field similar expressions are

$$\begin{aligned} \mathbf{H}^{(p)}(x, z, t) &= [\mathbf{H}_1^{(p)}(x, z, t) + \mathbf{H}_2^{(p)}(x, z, t)] \exp(ik_{0x}x - i\omega_0 t), \\ \mathbf{H}_j^{(p)}(x, z, t) &= \mathbf{e}_y \int_{-\infty}^{\infty} \int_{-\infty}^{\infty} B_j^{(p)}(K, \Omega, z) H_{\text{in}}(K, \Omega) \\ &\times \exp(iKx - i\Omega t) dK d\Omega, \end{aligned} \quad (29)$$

where

$$B_j^{(p)}(K, \Omega, z) = \exp(iq_{zj}^{(p)}z) \sum_{g=0,h} B_{gj}^{(p)} \exp(-igx).$$

Equations (22) and (27), or (28) and (29), describe the values of electric and magnetic fields of transmitted and diffracted waves in a PC layer of thickness z . As the output pulse in

a vacuum has equal amplitudes of electric and magnetic fields, $E_g(x, z, t) = H_g(x, z, t)$, therefore, Eqs. (22) and (27) can be used for calculation of electric field intensity of the pulses after their output from a PC.

3. DIPS EFFECT FOR DIFFERENT POLARIZED INCIDENT PULSES

Let us discuss now the dynamics of short laser pulses at the Laue scheme of the dynamical Bragg diffraction in a 1D PC and for an arbitrary orientation of the polarization plane of linearly polarized incident radiation. It will be demonstrated in this section that, under these conditions, the DIPS leads to the appearance of four pulses after passing through a 1D PC with optically isotropic layers, while only two pulses are expected to appear in the cases of *s*- or *p*-polarized laser beam [16–18].

It stems from Eqs. (13), (15), and (24) that dispersion laws for the *s*- and *p*-polarized waves are different:

$$q_{zj}^{(s,p)^2} = k^2\chi_0 - q_{0x}^2 + h\alpha_0 \mp \sqrt{h^2\alpha_0^2 + C^{(s,p)^2}\chi_h\chi_{-h}k^4}, \quad (30)$$

where $\alpha_0 = q_{0x} - h/2$. The polarization factor in Eq. (30) is a constant for the *s*-polarized field, $C^{(s)} = \sqrt{C_h C_{-h}} = 1$, while for the *p*-polarized field $C^{(p)}$ is a function of the frequency and of the structural parameters [Eq. (14)]:

$$C^{(p)^2}(\omega, q_{0x}) = 1 - h^2/\chi_0 k^2 + h^2(h - q_{0x})q_{0x}/\chi_0^2 k^4. \quad (31)$$

Figure 2 presents the dispersion curves $q_{zj}^{(s,p)}(q_{0x})$ that are the isofrequency sections of a PC dispersion surface. Each of the projections of the wave vector q_{0x} corresponds unambiguously to the angle of incidence shown on the upper axis of the figure. The normal to the dispersion curves shown by the arrows indicates the directions of the energy propagation, i.e., of the group velocity for the Borrmann and anti-Borrmann modes [19]. It can be seen that the dispersion curves of the two modes differ significantly.

The polarization dependence of the direction of the group velocity appears under the deviation of the incident beam propagation from the exact Bragg condition, $\alpha_0 \neq 0$. The corresponding wave amplitudes are presented in Fig. 3. It

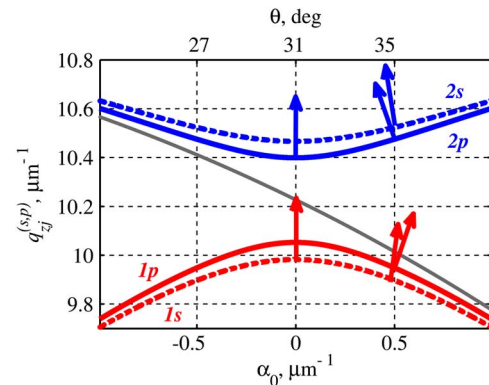


Fig. 2. Dispersion curves $q_{zj}^{(s,p)}(\alpha_0)$ for the Borrmann (red lines 1s, 1p) and anti-Borrmann (blue lines 2s, 2p) modes calculated by Eq. (30) for the *s*- (dashed lines) and *p*-polarized (solid lines) incident radiation, and for a homogeneous medium with the same value of the average refractive index n_a (gray line). The refractive indexes of the layers are: $n_1 = 1.445$ and $n_2 = 1.355$; $d = 775$ nm, $d_1/d = 0.5$, $\lambda_0 = 800$ nm, $\theta_B = 31^\circ$.

follows from Figs. 2 and 3 that the pulse propagation direction shown by arrows in Fig. 2 is determined by the ratio of the amplitudes of the transmitted and diffracted waves (Fig. 3). For example, for $\alpha_0 > 0$ the amplitude of transmitted wave of the Borrmann pulse is larger than the amplitude of the diffracted wave $|E_{01}| > |E_{h1}|$, then the pulse propagates in a forward direction with the wave vector \mathbf{q}_{01} (Fig. 2). At the same time, the anti-Borrmann pulse propagates in diffraction direction along wave vector \mathbf{q}_{h2} since $|E_{02}| < |E_{h2}|$.

It follows from the results shown in Fig. 2 that the effective refractive index of the anti-Borrmann eigenmode described by $n_{gj}^{(s,p)} = q_{gj}^{(s,p)}/k$ is larger for the *s*-polarized wave than for the *p*-polarized one, $n_{g2}^{(s)} > n_{g2}^{(p)}$. Vice versa, the ratio $n_{g1}^{(p)} > n_{g1}^{(s)}$ is valid for the case of the Borrmann mode. The Borrmann pulse fields $E_{g1}^{(s,p)}$ of both polarizations are localized in low-index layers, whereas anti-Borrmann mode $E_{g2}^{(s,p)}$ are localized in high-index layers, therefore, $n_{g1}^{(s,p)} < n_{g2}^{(s,p)}$ and $q_{z1}^{(s,p)} < q_{z2}^{(s,p)}$.

The difference in the group velocities of the *s*- and *p*-polarized pulses is caused not only by different values of the polarization factors $C^{(s,p)}$ but also by a large dispersion of the polarization factor $\partial C^{(p)}/\partial\omega \neq 0$ for the *p*-polarized pulse. Really, assuming the variable $q_{0x} = \text{const}$ in Eq. (30), the following expression for the *z* projection of the group velocity $v_z = (\partial q_z/\partial\omega)|_{q_{0x}}^{-1}$ can be obtained:

$$v_{zj}^{(s,p)} = c \frac{q_{zj}^{(s,p)}}{k} \left[\chi_0 \mp \frac{C^{(s,p)} \chi_h \chi_{-h} k^2 (2C^{(s,p)} + \omega \partial C^{(s,p)}/\partial\omega)}{2\sqrt{h^2 \alpha_0^2 + C^{(s,p)2} \chi_h \chi_{-h} k^4}} \right]^{-1}, \quad (32)$$

where $\partial C^{(s)}/\partial\omega = 0$ and the quantity $(\partial C^{(p)}/\partial\omega)|_{q_{0x}}$ is calculated from Eq. (31).

Figure 4 shows the dependencies of the group velocity projections on the detuning α_0 (actually on q_{0x}) described by Eq. (32) for the Borrmann ($j = 1$) and anti-Borrmann ($j = 2$) pulses of two polarizations. Here we assumed that a transversally unconfined pulse is incident on the PC boundary at a given angle θ_B , where θ_B is the Bragg angle for the central frequency of the pulse spectrum. It can be seen that all four group velocities $v_{z1,2}^{(s,p)}$ differ significantly from each other. Therefore, in a general case an incident laser pulse with an

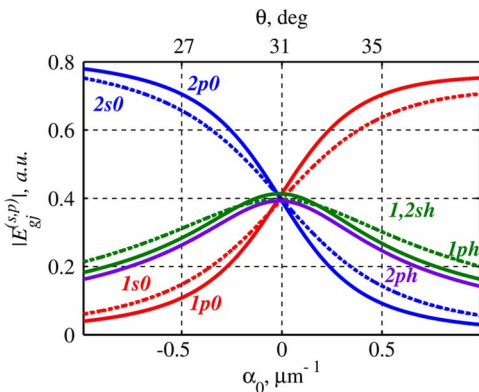


Fig. 3. Dependencies of the electric fields $|E_{gj}^{(s,p)}|$ on the detuning α_0 for the Borrmann (1) and anti-Borrmann (2) modes for the *s*- (dashed lines) and *p*-polarized (solid lines) incident radiation calculated by Eq. (26), and Eqs. (19) and (21), correspondingly. The parameters are the same as in Fig. 2.

arbitrary linear polarization is divided within PC into four pulses that propagate within the PC with different group velocities. Outside the PC four pulses propagate also in both transmission and diffraction directions.

A substantial role of different group velocities of eigenmodes in optical pulse splitting in a small array of silicon photonic wires at discrete diffraction was noted also in [20].

Let us define the time delay between the split Borrmann and anti-Borrmann pulses at a depth *z* inside the PC, or splitting time, as $t_{12}^{(s,p)} = z/v_{z1}^{(s,p)} - z/v_{z2}^{(s,p)}$. Using the expressions for the group velocities [Eq. (32)] at the exact Bragg condition $\alpha_0 = 0$ and in the case of small parameter $\sin^2 \theta_B/\chi_0 \ll 1$ the following simple relations are obtained:

$$\begin{aligned} t_{12}^{(s)} &= (z\chi/c\chi_0^{1/2})(1 - \sin^2 \theta_B/2\chi_0), \\ t_{12}^{(p)} &= (z\chi/c\chi_0^{1/2})(1 + 3\sin^2 \theta_B/2\chi_0). \end{aligned} \quad (33)$$

The efficiency of the DIPS effect can be described by the value pulse splitting length L_{DIPS} . This parameter is determined by the pulse path length at which the split pulses are spaced by the time interval $|t_1 - t_2| = 2\tau$, where τ is the pulse duration, $t_j = L_{\text{DIPS}}/v_{zj}$. It follows from Eqs. (33), that $L_{\text{DIPS}}^{(s)} = (2\tau c\chi_0^{1/2}/\chi)(1 - \sin^2 \theta_B/2\chi_0)^{-1}$ and

$$L_{\text{DIPS}}^{(p)}/L_{\text{DIPS}}^{(s)} = (1 - \sin^2 \theta_B/2\chi_0)/(1 + 3\sin^2 \theta_B/2\chi_0) < 1.$$

Therefore, our theory predicts that a *p*-polarized pulse splits faster and at smaller depth of the PC than the *s*-polarized one. The splitting lengths for a porous quartz sample described below are $L_{\text{DIPS}}^{(p)} = 0.22$ mm and $L_{\text{DIPS}}^{(s)} = 0.34$ mm if the pulse duration is 30 fs.

4. EXPERIMENTAL SETUP AND SAMPLE PREPARATION

Experiments were performed for 1D multilayered porous-quartz-based PCs. The samples were made by temperature annealing of porous silicon PC fabricated by the electrochemical etching technique described in detail elsewhere [21]. Briefly, a *p*-type Si(001) wafer of the resistivity of about $0.005 \Omega \cdot \text{cm}$ is used as an anode in a two-electrode electrochemical cell with a platinum wire as a cathode, the HF:ethanol solution being used as an electrolyte. Under such conditions, the formation of an array of parallel pores in the

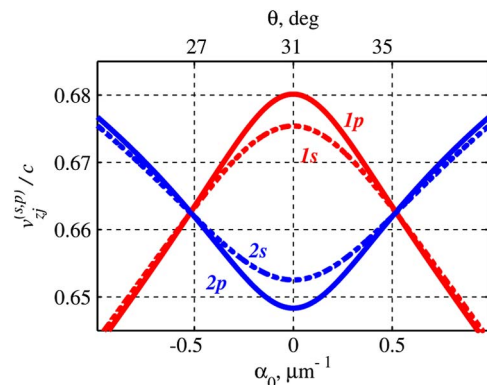


Fig. 4. Dependencies of the group velocity projections $v_{z1,2}^{(s,p)}$ Eq. (32) on the detuning α_0 . The parameters are the same as in Fig. 2.

silicon wafer and oriented along the [100] direction takes place, the diameter of pores being a linear function of the etching current density j . Spatial 1D periodicity of the structure is formed by the periodical in time modulation of j ($j_1 = 40 \text{ mA/cm}^2$ and $j_2 = 200 \text{ A/cm}^2$, respectively). In such a way, a porous-silicon 1D PC was formed with the thickness of each layer of 390 nm and with the period of 780 nm. We made the PC composed of 375 layers so that the total PC thickness of 300 μm was large enough for the performance of the experiments in the Laue geometry.

In order to make the multilayered structure transparent at the wavelength of 800 nm, the annealing of the porous silicon PC in an oven in an oxygen atmosphere and at the temperature of 900°C for 1–2 h was performed. As a result, the total oxidation of silicon in the structure and formation of a porous quartz multilayer structure was achieved. Complementary measurements performed for the s -polarized light have shown that the refractive indices of the layers of high and low porosity decreased as compared with porous silicon ones down to $n_1 = 1.45 \pm 0.02$ and $n_2 = 1.35 \pm 0.02$, while prior to the annealing these values were $n_1 = 1.80 \pm 0.05$ and $n_2 = 2.20 \pm 0.05$. The Bragg diffraction condition was satisfied for the 31° angle of incidence of radiation with a wavelength of 800 nm.

As the porous silica is a birefringent material [22], the refractive indices for the ordinary (“ o ”) and extraordinary (“ e ”) waves were measured in order to perform a full optical characterization of the structure. The measurements were performed for thick porous silica layers of a few microns thick with the same porosity as the layers in the described above PC and on porous substrate. The following values were obtained for the layers of low and high porosity: $n_{1,o} = 1.45 \pm 0.01$ and $n_{2,o} = 1.35 \pm 0.01$, $n_{1,e} = 1.43 \pm 0.01$ and $n_{2,e} = 1.32 \pm 0.01$, so the refraction index contrasts are $\delta_o = 0.10$ and $\delta_e = 0.11$, respectively.

After the annealing the PC was polished mechanically so that two different PC slabs (3.8 mm thick and 2 mm thick) of the dimensions 0.3 mm \times 3.8 mm \times 5 mm and 0.3 mm \times 2 mm \times 5 mm were formed; the two samples are denoted below as sample I and II, respectively.

For the experimental studies of the DIPS effect, the 110 fs and 30 fs light pulses at a wavelength of 800 nm generated by a Ti-sapphire laser were used, the repetition rate being 80 MHz. The maximal average power of the fundamental radiation was 100 mW. The laser beam was focused on the cut-off of the PC into a spot of approximately 30 μm in diameter at an angle of incidence of 31°, i.e., under the Bragg diffraction condition. The laser beam after passing through the PC at the Laue geometry was directed to an autocorrelometer and the second-order autocorrelation function was measured, similarly to that described in [18].

5. EXPERIMENTAL RESULTS AND DISCUSSION

Figures 5–7 show the second-order intensity autocorrelation functions measured for transmitted signals for the s - or p -polarizations of the incident pulsed radiation, as well as for a “mixed” polarization, when the polarization plane was tilted to 28° and 64° with respect to p -polarizations; in what follows it is denoted by the letter “ m .” It can be seen that

the autocorrelation functions change dramatically as the polarization of the pulsed laser radiation is varied.

Experimental autocorrelation functions of transmitted pulses were fitted by the following theoretical functions:

$$I_{AC}^{(s,p)}(\tau) = \int_{-\infty}^{\infty} I_0^{(s,p)}(t) I_0^{(s,p)}(t + \tau) dt, \quad (34)$$

where the field intensities

$$I_0^{(s)}(t) = |\mathbf{E}_0^{(s)}(t)|^2, \quad I_0^{(p)}(t) = |\mathbf{H}_0^{(p)}(t)|^2, \quad (35)$$

were calculated by Eqs. (27) and (22), respectively, in the point $x = 0$ and $z = L$. The incident pulse shape was described by a Gaussian function $E_{in}(x, t) = E_{in0} \exp[-(2x \cos \theta/D)^2 - (t - x \sin \theta/c)^2/\tau_0^2]$, where D is the input pulse transverse size and τ_0 is the pulse duration.

Figure 5 shows the results obtained for the longer sample I and for the incident pulse duration of 110 fs. The autocorrelation functions measured for the s -polarized and p -polarized fundamental beam reveal three strong peaks [Figs. 5(a) and 5(b)] that correspond to the temporal splitting of each of the incident pulse into two ones—Borrmann and anti-Borrmann pulses [Figs. 5(c) and 5(d)]. The time delays are $t_{12,o}^{(s)} = 804 \text{ fs}$ and $t_{12,e}^{(p)} = 1255 \text{ fs}$. As can be seen from the Figs. 5(a) and 5(b), the experimental autocorrelation functions are in a good agreement with the theoretical ones calculated by Eq. (34). The simple approximated formulas [Eq. (33)] give also good estimation for the time delays: $t_{12,o}^{(s)} = 826 \text{ fs}$ and $t_{12,e}^{(p)} = 1170 \text{ fs}$.

For the calculations we have taken into account the material birefringence of porous fused quartz [22] that conforms the PC structure. It is known that the porous quartz is a negative uniaxial material with the optical axis parallel to the pore direction. In the case of the PCs studied in our work, the optical axis is oriented along the normal to PC

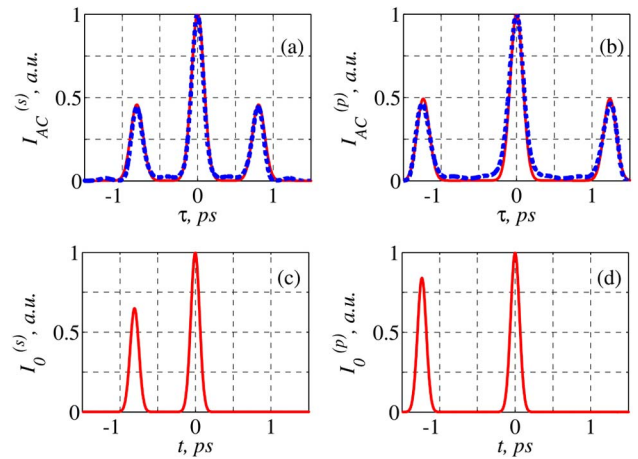


Fig. 5. Measured (blue dashed lines) and calculated by Eqs. (34) and (35) (red solid lines) intensity autocorrelation functions $I_{AC}(\tau)$ of laser pulses passed through the PC in the direction of the transmitted wave at (a) s -polarized incident pulse and (b) p -polarized one for sample I ($L = 3.8 \text{ mm}$). The time dependence of the calculated by Eq. (35) pulse intensities $I_0^{(s,p)}(t)$ that provide the best correlation with the experimental data for (c) s -polarized and (d) p -polarized incident pulse radiation. The refractive indexes of the layers are: $n_{1,o} = 1.455$, $n_{2,o} = 1.345$, $n_{1,e} = 1.440$, and $n_{2,e} = 1.320$; pulse duration is $\tau_0 = 110 \text{ fs}$.

layers. For the *s*-polarized laser beam, the electric field vector is perpendicular to the optical axis of the structure, so only the ordinary wave propagates within the PC. Otherwise, the electric field vector for the *p*-polarized beam lies in the plane of incidence. If this plane coincides with the principal optical plane of the PC, we will have only the extraordinary wave in the PC. Thus, we have to assume that the physical mechanisms of the polarization pulse splitting effect cannot be attributed simply to the birefringence effects in the porous silica PCs. The pulse splitting is a pure DIPS effect. The *p*-polarized extraordinary pulse splits faster than the *s*-polarized ordinary one and $t_{12,e}^{(p)} > t_{12,o}^{(s)}$ as the DIPS theory predicts, Eq. (33).

The experimental results of the autocorrelation function measured for the sample I in the case of the mixed plane polarization of the input and output radiation with different angles of polarization $\phi = 64^\circ$ and 28° are shown in Figs. 6(a) and 6(b). The angle $\phi = 0^\circ$ would correspond to pure *p*-polarized pulse. The approximation of these dependencies requires the existence of three pulses in the outgoing beam; the corresponding spatial profile of the intensity of the outgoing pulses is shown in Figs. 6(c) and 6(d).

The temporal profile of the intensity of the outgoing radiation in the case of *m*-input, *m*-output combination of polarizations becomes evident if we take into account that a mixed polarized field is a superposition of two orthogonally polarized waves and contains some parts of both *p*- and *s*-polarized fields, so the intensity is

$$I_0^{(m)}(t, \phi) = I_0^{(p)}(t) \cos^2(\phi) + I_0^{(s)}(t) \sin^2(\phi). \quad (36)$$

In a definite sense the experimental situation is intermediate between the two described previously, *s*-input, *s*-output and *p*-input, *p*-output. The specific splitting times being the same as estimated above (Fig. 5). As it follows Eq. (32) and Fig. 4 for the group velocities of the split pulses, in the general case of arbitrary pulse polarization four pulses in PC with different group velocities exist. However, the calculation

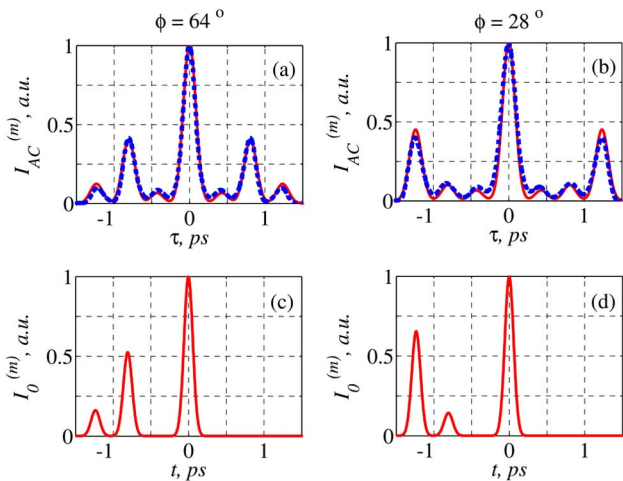


Fig. 6. (a), (b) Experimental (dashed lines) and calculated by Eq. (34) for $I_0^{(m)}$, Eq. (36) (solid lines) autocorrelation functions $I_{AC}^{(m)}(\tau)$ of the laser pulses passed through the PC in the direction of the transmitted wave for the “mixed” polarizations of the incident and outgoing pulses for sample I. The polarization angles are (a) $\phi = 64^\circ$ and (b) 28° . (c), (d) The intensity of the pulses calculated by Eqs. (35) and (36). Parameters are the same as in Fig. 5.

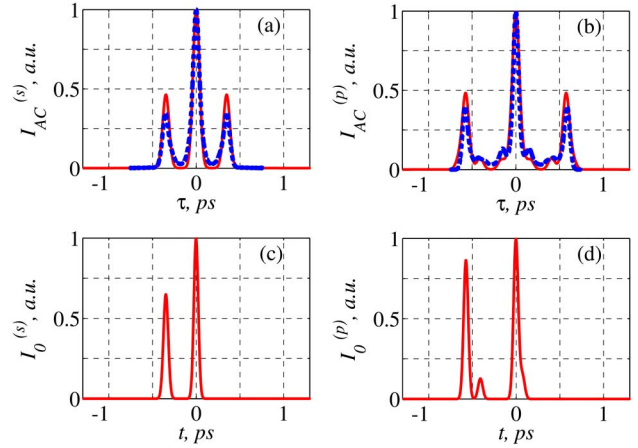


Fig. 7. Experimentally measured (blue dashed lines) and calculated by Eqs. (34) and (35) (red solid lines) intensity autocorrelation functions $I_{AC}(\tau)$ of laser pulses passed through the PC in the direction of the transmitted wave for (a) *s*-polarized incident pulse and (b) for the *p*-polarized pulses for the sample II with thickness $L = 2$ mm. The intensity of the pulses $I_0^{(s,p)}(t)$ calculated by Eq. (35) (c) for *s*-polarized incident pulse and (d) for *p*-polarized one. The PC parameters used in calculations are: for ordinary wave $n_{1,o} = 1.445$ and $n_{2,o} = 1.355$, for extraordinary $n_{1,e} = 1.433$ and $n_{2,e} = 1.327$; $d = 775$ nm, $d_1/d = 0.5$, $\lambda_0 = 800$ nm, $\theta = \theta_B = 31^\circ$, $\tau_0 = 30$ fs, $D = 30$ μ m.

of the velocities by Eqs. (32) under the conditions of our experimental sample parameters shows that the two velocities for anti-Bormann pulses have the same values $v_{22,o}^{(s)} = v_{22,e}^{(p)}$, and so we have only three pulses at the output and not four. The left peaks in Figs. 6(c) and 6(d) correspond to fast Bormann *p*-polarized pulses, the middle peaks are Bormann *s*-polarized pulses, and the right peaks are *p*- and *s*-polarized slow anti-Bormann pulses propagating with identical velocities. It is worth noting that the amplitudes of the three peaks are comparable. Thus, the observed effect of the polarization-sensitive temporal splitting of the femtosecond laser pulses allows for control over the number of outgoing from the PC pulses, as well as over their intensity and time delay.

Figure 7 shows the results obtained for the shorter sample II and for the incident pulse duration of 30 fs, which are in a qualitative agreement with those obtained for the sample I in the case of *s*-polarization. Three peaks in the autocorrelation function were observed [Fig. 7(a)], which correspond to the temporal splitting of each pulse into two ones [Fig. 7(c)] with splitting time $t_{12,o}^{(s)} = 350$ fs and is in a good agreement with theoretical results.

The autocorrelation function for the *p*-polarized pulse shown in Fig. 7(b) is much more complicated and reveals a fine structure—three strong peaks as well as four small ones. This picture corresponds evidently to the case when two pairs of pulses exist after passing through the PC structure, the splitting time in pairs of pulses being different [Fig. 7(d)]. The presence of the two strong pulses is in agreement with our previous work [18]. The observation of two weak pulses has not been done previously. In this work we register them due to an increased temporal resolution of the detection system, as 30 fs laser pulses are used instead of 110 fs ones. In the case of *p*-polarization, two characteristic values of the splitting time exist, which match with the existence of two pairs of split femtosecond pulses, which in turn correspond to the strong and weak peaks in the autocorrelation function. The

time shift between the light pulses that correspond to strong peaks in Fig. 7(b) is $t_{12,e}^{(p)} = 570$ fs, while for the weak peaks it is found to be 480 fs. Seemingly, the appearance of weak peaks in Fig. 7(b) is explained by small deviation of the plane of incidence from the principal optical plane of birefringent porous quartz PC in our experiment. In this case, a small projection of the electric field on the direction that is perpendicular to the principal optical plane exists, so the light within a PC has both extraordinary (large) and ordinary (small) components. Orientation of the extraordinary field component is close to p -polarized field in PC, and so the calculations using Eqs. (22) and (35) give a good coincidence with the experiment [large peaks in Figs. 7(b) and 7(d)]. For the small peaks our theory cannot give strict description, but it is interesting that the best correlation with the experimental data is provided if one uses Eqs. (22) and (35) for a p -polarized field with the refractive indices for the ordinary waves [small peaks in Figs. 7(b) and 7(d)].

The physical nature of the observed effect is diffraction. Really, this effect cannot be associated solely with the birefringence of the porous silica PC. The latter one does not result in the duplication of the number of pulses in the cases of p -input, p -output or of s -input, s -output combinations of polarizations. In our case we see the pulse splitting of both p -input and s -input pulses. The diffraction nature of the observed phenomenon is proved by a good agreement of the experimental data and DIPS theory. In accordance with Eq. (32) the large dispersion of polarization factor $C(\omega)$ for p -polarized pulse, which is explained by a lattice-induced dispersion in PC, plays the principal role in determining pulse group velocities and, as a result, of a splitting time value.

6. CONCLUSION

In conclusion, theoretical and experimental studies of the polarization effects in DIPS in 1D PCs at the Laue scheme of diffraction are performed. The experiments are performed for a multilayer fused quartz PC fabricated by the temperature annealing of porous silicon templates. We have demonstrated that a temporal splitting of femtosecond laser pulses is observed in the chosen experimental scheme and that the splitting time depends dramatically on the polarization of the laser pulses, being nearly twice as large for the p -polarization as compared with s -one. Moreover, for a mixed polarization the picture of the temporal splitting is more rich and demonstrates three time-shifted pulses. Experimental results are well described by linear DIPS theory for 1D PC. The theory explains the significant polarization effects in DIPS by a large lattice-induced dispersion of polarization factor. The DIPS effect can be observed also in high-quality 2D and 3D PCs under condition of the Laue scheme of the Bragg diffraction [23].

ACKNOWLEDGMENTS

This work was partially supported by the Russian Foundation for Basic Research, Grant No. 13-02-00300, and by the Federal Program of the Russian Ministry of Education and Science, Grant No. 8393.

REFERENCES

1. K. Busch, G. Von Freymann, S. Linder, S. Mingaleev, L. Tkeshelashvili, and M. Wegener, "Periodic nanostructures for photonics," *Phys. Rep.* **444**, 101–202 (2007).

2. Y. S. Kivshar and G. P. Agrawal, *Optical Solitons: From Fibers to Photonic Crystals* (Academic, 2003).
3. Y. V. Kartashov, B. A. Malomed, and L. Torner, "Solitons in nonlinear lattices," *Rev. Mod. Phys.* **83**, 247–305 (2011).
4. P. Yeh, A. Yariv, and C. Hong, "Electromagnetic propagation in periodic stratified media. I. General theory," *J. Opt. Soc. Am.* **67**, 423–438 (1977).
5. H. Gersen, T. J. Karle, R. J. Engelen, W. Bogaerts, J. P. Korterik, N. F. van Hulst, T. F. Krauss, and L. Kuipers, "Real-space observation of ultraslow light in photonic crystal waveguides," *Phys. Rev. Lett.* **94**, 073903 (2005).
6. H. Altug and J. Vuckovic, "Experimental demonstration of the slow group velocity of light in two-dimensional coupled photonic crystal microcavity arrays," *Appl. Phys. Lett.* **86**, 111102 (2005).
7. A. Belardini, O. Baganov, G. Leahu, A. Dosco, M. Centini, E. Fazio, C. Sibilia, M. Bertolotti, S. Zhukovsky, and S. Gaponenko, "Dynamic response of a coupled-cavities one-dimensional photonic crystal in the femtosecond regime," *J. Optoelectron. Adv. Mater.* **8**, 2015–2017 (2006).
8. M. Scalora, M. J. Bloemer, A. S. Manka, J. P. Dowling, C. M. Bowden, R. Viswanathan, and J. W. Haus, "Pulsed second-harmonic generation in nonlinear one-dimensional periodic structures," *Phys. Rev. A* **56**, 3166–3174 (1997).
9. A. V. Balakin, V. A. Bushuev, B. I. Mantsyzov, I. A. Ozheredov, E. V. Petrov, A. P. Shkurinov, P. Masselin, and G. Mouret, "Enhancement of sum frequency generation near the photonic band gap edge under the quasi-phase-matching conditions," *Phys. Rev. E* **63**, 046609 (2001).
10. M. Loncar, T. Yoshie, A. Scherer, P. Gogna, and Y. Qiu, "Low-threshold photonic crystal laser," *Appl. Phys. Lett.* **81**, 2680–2682 (2002).
11. J. T. Mok, C. M. deSterke, and B. J. Eggleton, "Delay-tunable gap-soliton-based slow-light system," *Opt. Express* **14**, 11987–11996 (2006).
12. M. Calvo, P. Cheben, O. Martinez-Matos, F. del Monte, and J. A. Rodrigo, "Experimental detection of the optical Pedellossung effect," *Phys. Rev. Lett.* **97**, 084801 (2006).
13. B. Terhalle, A. Desyatnikov, D. Neshev, W. Krolikowski, C. Denz, and Y. S. Kivshar, "Dynamic diffraction and interband transition in two-dimensional photonic lattices," *Phys. Rev. Lett.* **106**, 083902 (2011).
14. S. Savo, E. Di Gennaro, C. Miletto, A. Andreone, P. Dardano, L. Moretti, and V. Mocella, "Pendellosung effect in photonic crystals," *Opt. Express* **16**, 9097–9105 (2008).
15. A. Balestreri, L. C. Andreani, and M. Agio, "Optical properties and diffraction effects in opal photonic crystals," *Phys. Rev. E* **74**, 036603 (2006).
16. V. A. Bushuev and B. I. Mantsyzov, "Linear effect of doubling of the laser pulse repetition rate in the Laue geometry of Bragg diffraction in a photonic crystal," *Bull. Russ. Acad. Sci.: Phys.* **72**, 30–34 (2008).
17. A. A. Skorynin, V. A. Bushuev, and B. I. Mantsyzov, "Dynamical Bragg diffraction of optical pulses in photonic crystals in the Laue geometry: diffraction-induced splitting, selective compression, and focusing of pulses," *JETP* **115**, 56–67 (2012).
18. S. E. Svyakhovskiy, V. O. Kompanets, A. I. Maidikovskiy, T. V. Murzina, S. V. Chekalin, V. A. Bushuev, A. A. Skorynin, and B. I. Mantsyzov, "Observation of diffraction-induced laser pulse splitting in a photonic crystal," *Phys. Rev. A* **86**, 013843 (2012).
19. Z. G. Pinsker, *Dynamical Scattering of X-rays in Crystals*, Vol. 3 of Springer Series On Solid-State Science (Springer, 1977).
20. C. J. Benton and D. V. Skryabin, "Coupling induced anomalous group velocity dispersion in nonlinear arrays of silicon photonic wires," *Opt. Express* **17**, 5879–5884 (2009).
21. S. E. Svyakhovskiy, A. I. Maydykovsky, and T. V. Murzina, "Mesoporous silicon photonic structures of thousands of periods," *J. Appl. Phys.* **112**, 013106 (2012).
22. L. A. Golovan, V. A. Melnikov, S. O. Konorov, A. B. Fedotov, V. Y. Timoshenko, A. M. Zheltikov, P. K. Kashkarov, D. A. Ivanov, G. I. Petrov, and V. V. Yakovlev, "Linear and nonlinear optical anisotropy of amorphous oxidized silicon films induced by a network of pores," *Phys. Rev. B* **73**, 115337 (2006).
23. B. Bruser, I. Staude, G. Freymann, M. Wegener, and U. Pietsch, "Visible light Laue diffraction from woodpile photonic crystals," *Appl. Opt.* **51**, 6732–6737 (2012).